Two-phase flow induced vibrations in a marine riser conveying a fluid with rectangular pulse train mass

José Manuel Cabrera-Miranda [a,b], Jeom Kee Paik [a,b,c]*

[a] *Department of Naval Architecture and Ocean Engineering, Pusan National University, Busan 46241, Republic of Korea*

[b] *The Korea Ship and Offshore Research Institute (The Lloyd's Register Foundation Research Centre of Excellence), Pusan National University, Busan 46241, Republic of Korea*

[c] *Department of Mechanical Engineering, University College London, London WC1E 7JE, UK*

* Corresponding Author. J.K. Paik. Tel: +82 51 510 2429, Mobile: +82 10 3853 8757, Fax: +82 51 518 7687

E-mail addresses: cabrera@pusan.ac.kr (J.M. Cabrera-Miranda), jeompaik@pusan.ac.kr (J.K. Paik).

Abstract

A riser conveys fluids from a subsea system to a host floater; however, oil and gas phases may alternate, increasing pipe's stress and damaging downstream facilities. This paper studies the nonlinear planar vibrations of a steel lazy wave riser excited by slug flow. The employed formulations comprise the Euler-Bernoulli beam model and the steady plug-flow model with a time-space-varying mass per unit length in the form of a rectangular pulse train. The equations are solved by a Runge-Kutta finite difference scheme and frequency-response curves are constructed for effective tension, curvature, usage factor and fatigue damage. The results offer a useful insight of the slugging frequencies and slug lengths that may receive attention during the design of risers.

Keywords: steel lazy wave riser (SLWR); curved pipe conveying fluid; two-phase flow-induced vibration; time-varying mass parametric vibration; ultimate limit state (ULS); cumulative fatigue damage.

Nomenclature

a	gas to liquid density ratio
A_f	internal fluid's cross-sectional area [m^2]
A_p	pipe's structural cross-sectional area [m^2]
$\mathcal{A}$	dimensionless pipe's structural cross-sectional area
C_a	added mass coefficient
C_d	drag coefficient in normal direction
C_{dt}	drag coefficient in tangential direction
D	structural diameter [m]
D_o	outer diameter to account for hydrodynamic forces [m]
$\mathcal{D}$	accumulated fatigue damage
E	Young's modulus of the pipe [Pa]
e	axial strain due to tension

f frequency [s^{-1}]
f_l slugging frequency [s^{-1}]
g acceleration of gravity [$m \cdot s^{-2}$]
h pipe wall thickness [m]
I area moment of inertia of the pipe [m^4]
L unstretched pipe length [m]
M mass of internal fluid [$kg \cdot m^{-1}$]
m mass per unit length of the pipe element [$kg \cdot m^{-1}$]
m_a added mass per unit length [$kg \cdot m^{-1}$]
m_b mass per unit length of the buoyancy modules [$kg \cdot m^{-1}$]
m_m mass of the marine growth [$kg \cdot m^{-1}$]
m_p mass per unit length of the bare pipe [$kg \cdot m^{-1}$]
$\mathcal{M}$ bending moment [N·m]
$\mathcal{M}_k$ plastic bending moment resistance [N·m]
N_i number of cycles to failure at constant stress range
n_i number of cycles in stress block i
p pipe's tangential displacement [m]
p_c hoop buckling capacity [Pa]
p_b burst resistance [Pa]
p_e external pressure [Pa]
p_i internal pressure [Pa]
q pipe's normal displacement [m]
s local curvilinear Lagrangian coordinate [m]
S_n in-plane shear force [N]
$\mathcal{S}$ principal stress in axial direction [Pa]
T pipe's tension accounting for hydrostatic pressure effects [N]
t time [s]
T_e pipe's effective tension [N]
T_k plastic axial force resistance [N]
U internal fluid's axial velocity [$m \cdot s^{-1}$]
u pipe's tangential velocity [$m \cdot s^{-1}$]
$\mathcal{U}$ dimensionless internal fluid's axial velocity
v pipe's normal velocity [$m \cdot s^{-1}$]
w_0 submerged weight per unit length of pipe [$N \cdot m^{-1}$]
w_1 dimensionless tangential velocity
w_2 dimensionless normal velocity
x abscissa [m]
y ordinate [m]
α dimensionless mass of internal liquid
β dimensionless pipe's submerged weight

γ dimensionless internal fluid's weight
ζ dimensionless Lagrangian coordinate
ζ^* dimensionless stretched curvilinear coordinate
λ dimensionless wavelength
λ_l dimensionless length of liquid slug
η_1 dimensionless tangential displacement
η_2 dimensionless normal displacement
μ dimensionless drag area
ν dimensionless added mass
ρ density of the surrounding fluid [$kg \cdot m^{-3}$]
ρ_l density of the conveyed fluid liquid phase [$kg \cdot m^{-3}$]
ς dimensionless mass of buoyancy modules
τ dimensionless time
υ usage factor
ϕ angle formed between the tangent of the pipe and the horizontal plane of reference [rad]
χ dimensionless effective tension
Ψ pulse train function
Ω_3 pipe's curvature [m^{-1}]

1. Introduction

A riser is an important interface between a subsea system and its host platform in the exploration and production of offshore hydrocarbons. A type of riser, the steel lazy wave riser (SLWR) has been proven over the past few years as a cost effective solution for the production of fields in ultra-deep water and harsh environment (Hoffman et al., 2010; Moore et al., 2017). Buoyancy modules are distributed at its middle length in order to keep its compliant configuration, isolating floater motions from the touch down zone, and hence, improving the fatigue life (Felisita et al., 2017). Furthermore, it is made of steel pipe, which is a suitable material for the exploitation of high pressure and high temperature reservoirs (Cheng and Cao, 2013).

It has been recognised that the slug flow regime inside SLWRs could be an issue, especially at the sag section where liquids could be accumulated (Kim and Kim, 2015). Accordingly, two-phase flow-induced vibration (2-FIV) or slug-induced vibration can occur, diminishing the risers fatigue life (Cheng and Cao, 2013).

Slug flow is a phenomenon in which liquid "slugs" and gas "bubbles" of a two-phase flow alternate in the pipe. This may result in parametric vibrations due to the time-varying mass in the form of a square wave (Paidoussis, 2014) which could resonate with the structural system (Chatjigeorgiou, 2017). In the oil and gas industry, the slug flow pattern hinders the operations of downstream facilities (Kadri et al., 2011; Li et al., 2017) and the induced vibrations increase the fatigue damage of piping systems (van der Heijden et al., 2014). Hence, methods to mitigate the slugging, such as using a wavy pipe (Xing et al., 2013) or a self-lifting arrangement (Adefemi et al., 2017), have been proposed. Furthermore, 2-FIV occurs in other hydraulic systems, such as spiral pipes conveying boiling liquid in heat exchangers (Gulyayev and Tolbatov, 2004; Yan et al., 2013), at the outlet of steam generators, in piping of nuclear power plants (Fujita, 1990; Ortiz-Vidal et al., 2017), in parallel pipes for direct steam generation by solar heating (Tshuva et al., 1999) and in aspirating pipes with density pulsations due to shallow immersion (Paidoussis, 2014).

Several papers have focused on the slug flow characterisation. Numerical and experimental methods have been applied to study inclined pipeline-riser systems (Han and Guo, 2015), vertical risers (Abdulkadir et al., 2014; Fokin et al., 2006) and hybrid risers (Gong et al., 2014). The experiments on an s-shaped riser are of particular interest for this paper; they have been conducted inside a stainless steel pipeline-riser system with a gas-liquid mixer, and the observations have helped to develop of a stability criteria for the flow (Li et al., 2017).

Concerning the 2-FIV, early experiments with air-water flow may be attributed to Hara (1977), and Hara and Yamashita (1978), where parametric vibrations were found owing to density fluctuations. Miwa et al. (2015) have written a comprehensive review on the 2-FIV, mainly with references earlier than 2014. While the Euler-Bernoulli is often adopted to study the 2-FIV (An and Su, 2015; Bai et al., 2018; Ortiz-Vidal et al., 2017; van der Heijden et al., 2014; L. Wang et al., 2018), using the Timoshenko beam model yields in the prediction of higher response amplitude when the system is about to lose stability (Ma et al., 2017). In other studies, experiments have been often used to validate the predictions by the beam models (Ortiz-Vidal et al., 2017; L. Wang et al., 2018). Furthermore, with the advent of high performance computing, computational fluid dynamics (CFD) coupled with finite element method (FEM) codes have been used to solve fluid-structure interaction (FSI) problems in subsea pipeline systems (Jia, 2012; Li et al., 2016; Lu et al., 2016; Onuoha et al., 2018, 2016).

Limiting the discussion to 2-FIV in marine compliant risers, Ortega et al. (2012) used a Lagrangian tracking model two-phase flow code coupled with a FEM code in order to solve planar motions of a flexible lazy wave riser, and they found that the irregular characteristics of the slug flow generate irregular loads and responses of the structure. Later, Ortega et al. (2017) included wave loads into their model, and the riser's response got amplified. Chatjigeorgiou (2017) analysed the linearised in-plane motions of a catenary riser conveying a steady slug-flow and subjected to forced top excitation. It was concluded that the said flow amplifies the dynamic components of the riser's response. Recently, Zhu et al. (2018) performed experiments in an air-water test loop, where the in-plane vibrations, out-of-plane vibrations and the flow structure were observed inside a transparent silica gel tube in catenary configuration by means of high speed cameras. Results showed that the lateral vibrations are negligible, and hence, the idea of using planar motion models seems to be a plausible

approximation. Furthermore, a number of useful contributions to the analysis and design of marine risers or pipelines are available in the literature published in recent years (Ai et al., 2018; Lou et al., 2017; Park et al., 2015; Yuan et al., 2018; Khan and Ahmad, 2017; Li and Low, 2012; Guo et al., 2013; Wang et al., 2018; Gao et al., 2014; Gao et al., 2016; Xu et al., 2017; Bai et al., 2017; Bai et al., 2018; Zhang et al., 2015; Ye et al., 2014; Dong et al., 2013; Wang et al., 2018; Katifeoglou and Chatjigeorgiou, 2016; Park et al., 2018; Vendhan, 2014; Gu et al., 2017).

The aim of this paper is to understand how the riser behaves before the time-varying mass of the slug flow, and whether the response is high enough to be considered in the structural design. To that end, a phenomenological model of the slug flow is used, namely a plug-flow model with time-space-varying mass in the form of rectangular pulse train, whereas the structure is modelled as an Euler-Bernoulli beam. In our application of interest, no floater motions are included, and the surrounding seawater is quiescent, providing only added mass and drag damping. By conducting a numerical study, we detect the slugging frequencies that may lead the riser to attain the ultimate limit state (ULS) or cause major damage for the fatigue limit state (FLS).

Scholars of the International Ship and Offshore Structures Congress (ISSC) have identified that the research of loads on risers should focus on the development of simplified methods for use in practical design applications (Hirdaris et al., 2014), and this paper is aligned towards that objective. The rectangular pulse train mass model here used assumes a known varying mass across the riser, and therefore, it is considerably simpler than the aforementioned methods which require solving the fluid equations. Moreover, the said rectangular pulse train mass model has been used successfully in the past in the analysis of jumpers for subsea piping systems, where vibrations were predicted in a realistic way (van

der Heijden et al., 2014). Accordingly, this article offers two main contributions: (1) a mathematical model which can be used to benchmark more complex solutions that consider rigorous FSI models, and (2) an assessment on the relevance of 2-FIV for the limit state design of risers.

Although the present work focuses on SLWRs, the governing equations are general for elastic extensible pipes conveying fluid, and thus, the present approach can be applied to analyse other types of hydraulic systems by selecting the appropriate boundary conditions, tube properties and internal flow parameters.

Regarding the organisation of the paper, Section 2 introduces the governing system of equations and the numerical methods used to investigate the problem. Section 3 presents the numerical results of riser's response as function of slugging frequency and slug length. In section 4, we analyse the time histories of the said responses to assess the ULS and FLS. Conclusions are given in Section 5.

2. Mathematical model

2.1 Governing equations

In this study, an extensible riser conveying a fluid in still seawater is considered as depicted in Fig. 1. The Euler-Bernoulli beam model is used for the pipe element, the plug-flow model applies for the internal fluid, and the following assumptions are followed:

(i) The beam cross section in normal direction keeps straight and normal before and after deformation.

(ii) The rotational inertia of the beam is neglected, whereas inertial forces along normal and tangential directions are taken into account.

(iii) The pipe is extensible following a linear stress-strain relationship.

(iv) The structural cross-sectional area of the pipe is constant.

(v) The riser's response in the out-of-plane direction is neglected.

(vi) The location of the touchdown point (TDP) is constant, and hence, the soil-structure interaction and flowline section are neglected.

(vii) The internal flow is treated as an infinitely flexible rod travelling through the pipe, with all points of the fluid having constant velocity relative to the pipe, i.e. the flow is steady.

(viii) The slug-flow is modelled by a fluid with time-varying density in the form of a rectangular impulse train.

(ix) The drag force of the surrounding fluid in the tangential direction is neglected.

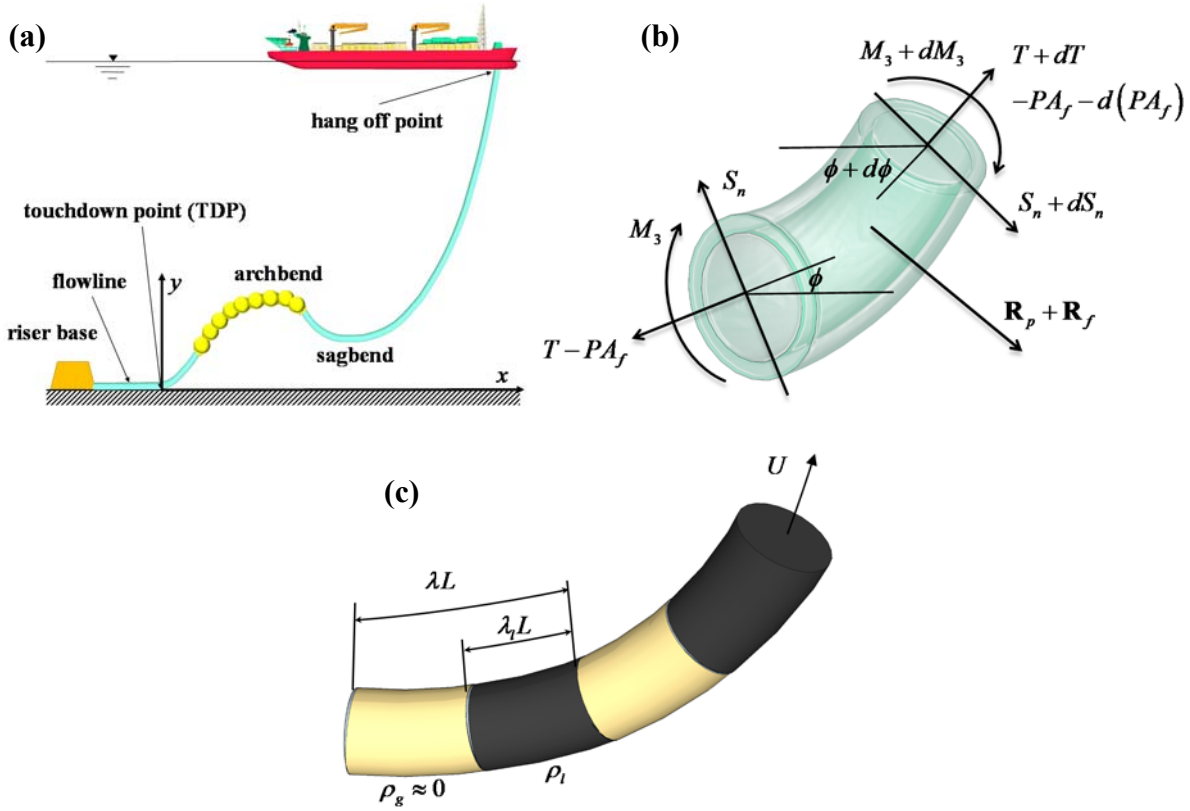

Fig. 1. Riser subjected to two-phase flow induced vibrations: **(a)** sketch of steel lazy wave riser, **(b)** in-plane balance of forces and moments acting on a pipe conveying fluid after elongation (M_3, $\mathbf{R}_p$ and $\mathbf{R}_f$ stand for moment around bi-normal axis, distributed forces applied on the pipe and distributed forces applied on the fluid element, respectively) and **(c)** internal fluid with time-space-varying mass in the form of a rectangular pulse train.

Accordingly, the planar motions of the riser can be described by the following set of partial differential equations (Chatjigeorgiou, 2017):

$$\begin{aligned} & m\frac{\partial u}{\partial t}-(m+M)\frac{\partial \phi}{\partial t}v+\frac{MU}{(1+e)}\left(\frac{\partial U}{\partial s}-\Omega_3 v\right) \\ & =\frac{\partial T_e}{\partial s}-S_n\Omega_3-(w_0+Mg)\sin\phi-\frac{1}{2}\pi\rho D_o C_{dt}u|u|\sqrt{1+e}, \end{aligned} \tag{1}$$

$$\begin{aligned} & (m+m_a+M)\frac{\partial v}{\partial t}+m\frac{\partial \phi}{\partial t}u+\frac{MU}{(1+e)}\left(\frac{\partial v}{\partial s}+\Omega_3 U\right) \\ & =\frac{\partial S_n}{\partial s}+\Omega_3 T_e-(w_0+Mg)\cos\phi-\frac{1}{2}\rho D_o C_d v|v|\sqrt{1+e}, \end{aligned} \tag{2}$$

$$\frac{1}{EA_p}\frac{\partial T_e}{\partial t}=\frac{\partial u}{\partial s}-\Omega_3 v, \tag{3}$$

$$\left(1+e\right)\frac{\partial \phi}{\partial t}=\frac{\partial v}{\partial s}+\Omega_3 u, \tag{4}$$

$$EI\frac{\partial \Omega_3}{\partial s}+S_n\left(1+e\right)^3=0, \tag{5}$$

$$\frac{\partial \phi}{\partial s}-\Omega_3=0, \tag{6}$$

where t is time, s is the local curvilinear Lagrangian coordinate that takes values along the unstretched pipe of length L, $M\left(t,s,\rho_l\right)$ is the mass of the fluid in the pipe, ρ_l is the density of the conveyed fluid liquid phase, $m\left(s\right)=m_p+m_b\left(s\right)+m_m\left(s\right)$ is the mass per unit length of the pipe element, m_p is the mass per unit length of the bare pipe including coating, $m_b\left(s\right)$ is the mass per unit length of the buoyancy modules which is zero outside the buoyancy section, $m_m\left(s\right)$ is the mass of the marine growth which is neglected in this paper for simplicity of the problem, $m_a\left(s\right)=C_a\left(\pi/4\right)\rho D_o\left(s\right)^2$ is the added mass of the surrounding fluid per unit length, C_a is the added mass coefficient, ρ is the density of the surrounding fluid, $D_o\left(s\right)$ is the outer diameter to account for hydrodynamic forces, $u\left(t,s\right)$ is the velocity of the pipe in the tangential direction of the pipe element, $v\left(t,s\right)$ is the velocity of the pipe in the normal direction, U is the fluid's velocity inside the pipe in the axial direction, $\phi\left(t,s\right)$ is the angle formed between the tangent of the pipe and the horizontal plane of reference, $\Omega_3\left(t,s\right)$ is the curvature of the pipe associated with the Euler angle of rotation around the bi-normal axis, $e\left(t,s\right)$ is the axial strain due to tension, A_f is the area occupied by the internal fluid, A_p is

the structural cross-sectional area of the pipe, I is the area moment of inertia of the pipe, E is the Young's modulus of elasticity of the pipe, $T_e(t,s) = T(t,s) - p_i(t,s)A_p$ is the effective tension, $T(t,s)$ is the tension of the pipe accounting for hydrostatic pressure effects, $p_i(t,s)$ is the internal pressure of the pipe, $S_n(t,s)$ is the in-plane shear force of the pipe, $w_0(s)$ is the submerged weight per unit length of the pipe, g is the acceleration of gravity, $C_{dt}(s)$ is the drag coefficient in tangential direction here taken as zero, and $C_d(s)$ is the drag coefficient in normal direction.

Equations (1)-(6) represent the balance of forces in axial direction, balance of forces in normal direction, compatibility relation of the pipe in axial direction, compatibility relation of the pipe in normal direction, balance of moments around the bi-normal axis, and the definition of curvature expressed by Euler angles, respectively.

Regarding the assumption (vii), time derivatives of internal fluid's mass, pressure and velocity have vanished in Eqs. (1)-(6) as consequence of the steady flow. Moreover, disregarding the rotational inertia in assumption (ii) may look unwise, since studies have shown the importance of this term, especially for thick beams (Hirdaris and Lees, 2005). Notwithstanding, the rotational inertia is considerably smaller than the bending stiffness for slender structures such as risers. For instance, the ratio of rotational inertia to bending stiffness for the riser analysed in Section 3 is in the order of 10^{-7}. Therefore, assumption (ii) has been applied in the derivation of Eq. (5) without losing accuracy in the calculations.

A rigorous derivation of the above mentioned system has been presented by Chatjigeorgiou (2010a, 2010b). Though axial strain is here considered, further simplification can be achieved by neglecting the riser's extensibility (J. Wang et al., 2018).

2.2 Dimensionless form

2.2.1 Nonlinear system

For convenience of the problem, the riser displacements p and q in the tangential and normal directions, respectively, are introduced together with the following dimensionless quantities:

$$\begin{aligned}
&\tau = tL^{-2}\left(EI/m_p\right)^{1/2},\ \zeta = s/L,\ \eta_1 = p/L,\ \eta_2 = q/L,\ w_1 = uL\left[m_p/(EI)\right]^{1/2},\\
&w_2 = vL\left[m_p/(EI)\right]^{1/2},\ \varsigma = m_b/m_p,\ \chi = T_e L^2/(EI),\ \mathcal{U} = UL\left[m_p/(EI)\right]^{1/2},\\
&\alpha = \rho_l A_f/m_p,\ \beta = w_0 L^3/(EI),\ \gamma = \rho_l A_f g L^3/(EI),\ \nu = C_a \pi \rho D_o{}^2/(4m_p),\\
&\mu = \rho D_o L/(2m_p),\ \mathcal{A} = A_p L^2/I,\ e = \mathcal{T}/\mathcal{A},
\end{aligned} \tag{7}$$

where the linear stress-strain relation has been followed.

Equations. (4)-(6) are substituted into Eqs. (1)-(3) and the system is then supplemented with Eq. (4) as well as with the definitions of the velocity in the tangential and normal directions. The resulting dimensionless form of the system of partial differential equations reads:

$$\dot{\eta}_1 = w_1, \tag{8}$$

$$\dot{w}_1 = (1+\varsigma)^{-1}\begin{bmatrix}\chi' + (1+e)^{-3}\phi''\phi' - (\beta+\gamma\Psi)\sin\phi + (1+e)^{-1}(1+\alpha\Psi)w_2' w_2\\ +(1+e)^{-1}(1+\alpha\Psi)\phi' w_1 w_2 + (1+e)^{-1}\alpha\Psi\mathcal{U}\phi' w_2\end{bmatrix}, \tag{9}$$

$$\dot{\eta}_2 = w_2, \tag{10}$$

$$\begin{aligned}
&\dot{w}_2 = (1+\alpha\Psi+\varsigma+\nu)^{-1}\\
&\cdot\begin{bmatrix}-(1+e)^{-3}\phi''' + \chi\phi' - (\beta+\gamma\Psi)\cos\phi - (1+e)^{1/2}\mu C_d w_2|w_2| - (1+e)^{-1}w_2' w_1\\ -(1+e)^{-1}\phi' w_1{}^2 - (1+e)^{-1}\alpha\Psi\mathcal{U}w_2' - (1+e)^{-1}\alpha\Psi\mathcal{U}^2\phi'\end{bmatrix},
\end{aligned} \tag{11}$$

$$\dot{\chi} = \mathcal{A}\left(w_1' - \phi' w_2\right), \tag{12}$$

$$\dot{\phi} = \left(1+e\right)^{-1}\left(w_2' + \phi' w_1\right), \tag{13}$$

where the dot and the prime denote differentiation with respect to τ and ζ, respectively, and $\Psi\left(\tau,\zeta\right)$ is the known pulse train function.

Regarding the boundary conditions of the SLWR in Fig. 1(a), the bottom end of the riser is the TDP, where soil-structure interaction is disregarded, whereas the top end is connected to a floater via an articulated connection. Since no floater motions are analysed, velocities and curvatures at both ends are assumed to be zero. The resulting six boundary conditions are given by

$$w_1\left(\tau,0\right) = w_2\left(\tau,0\right) = \phi'\left(\tau,\zeta\right)\big|_{\zeta=0} = w_1\left(\tau,1\right) = w_2\left(\tau,1\right) = \phi'\left(\tau,\zeta\right)\big|_{\zeta=1} = 0. \tag{14}$$

2.2.2 Time-space-varying mass

In order to investigate the effect of slug-flow in the riser's response, the mass per unit length of the internal fluid is multiplied by a known function $\Psi\left(\tau,\zeta\right)$. As seen in Fig. 1(c), the maximum fluid's density is that of the liquid slug in which Ψ becomes one, while the minimum is zero at the gas bubble in which Ψ becomes zero. Moreover, the density wave travels at constant speed relative to the pipe U (or $\mathcal{U}$ in its dimensionless form). Subsequently, the pulse train function can be expressed as the summation of rectangular pulses, given by

$$\Psi\left(\tau,\zeta^*\right) = \left(1+e\right)^{-1}\sum \Psi_j\left(\tau,\zeta^*\right), \tag{15}$$

$$\Psi_j(\tau,\zeta^*)=\begin{cases}a, & |\zeta^*-\upsilon\tau-j\lambda|>\lambda_l/2\\ 1, & |\zeta^*-\upsilon\tau-j\lambda|\le\lambda_l/2\end{cases}, \tag{16}$$

where ζ^* is the dimensionless stretched curvilinear coordinate of the pipe, λ is the wavelength of the pulse (length of liquid slug plus gas bubble) normalised respect to L, λ_l is the normalised length of the liquid slug and a is the gas to liquid density ratio (taken as zero in this paper after neglecting the modest density of the gas phase). One should note that $\Psi(\tau,\zeta^*)$ must be converted to $\Psi(\tau,\zeta)$ before incorporating it into the numerical solution.

2.3 Numerical solution

The system of Eqs. (8)-(14) is solved numerically by applying the finite difference method (FDM) and the Runge-Kutta method. This includes the discretisation in space by applying the difference operators with second order approximation, and then the resulting first order ordinary differential equations are solved by means of the 'ode45' Matlab function with an automatic step size. Details regarding Runge-Kutta-FDM numerical solution schemes have been presented elsewhere (Cabrera-Miranda and Paik, 2018; Kuiper et al., 2008) and other FDM schemes for the dynamic analysis of risers have been discussed in other papers (Chatjigeorgiou, 2008; J. Wang et al., 2018). Furthermore, it is worth to mention that the pulse train function $\Psi(\tau,\zeta^*)$ has been applied by using the Matlab's 'pulstran' function.

3. Numerical analysis

A hypothetical SLWR is considered with properties taken from the literature (Felisita et al., 2017). The riser is made of an X65 steel grade pipe, having 254 mm inner diameter, 26

mm wall thickness and a length of 2640 m for the suspended section before stretching. It is located in 2000 m water depth and the hang-off point is placed just 20 m below the sea level. The associated parameters are shown in Table 1. The overall procedure for analysis is illustrated in Fig. 2.

Table 1. Riser parameters.

L	2.641×10^{3} m
buoyancy section	$s\in[41,641]$ m
A_f	5.07×10^{-2} m^2
A_p	2.29×10^{-2} m^2
E	2.07×10^{11} Pa
I	2.26×10^{-4} m^4
w_0	$\begin{cases}-6.47\times10^{2}\ \mathrm{N\cdot m^{-1}} & \text{for buoyancy section}\\ 7.298\times10^{2}\ \mathrm{N\cdot m^{-1}} & \text{otherwise}\end{cases}$
ρ	1.025×10^{3} kg·m^{-3}
ρ_l	8×10^{2} kg·m^{-3}
D_o	4.584×10^{-1} m
C_a	1
C_d	0.9
ς	$\begin{cases}7.585\times10^{-1} & \text{for buoyancy section}\\ 0 & \text{otherwise}\end{cases}$
α	1.664×10^{-1}
β	$\begin{cases}-2.548\times10^{5} & \text{for buoyancy section}\\ 2.873\times10^{5} & \text{otherwise}\end{cases}$
γ	1.565×10^{5}
μ	$\begin{cases}4.646\times10^{3} & \text{for buoyancy section}\\ 2.547\times10^{3} & \text{otherwise}\end{cases}$
$\mathcal{A}$	7.056×10^{8}

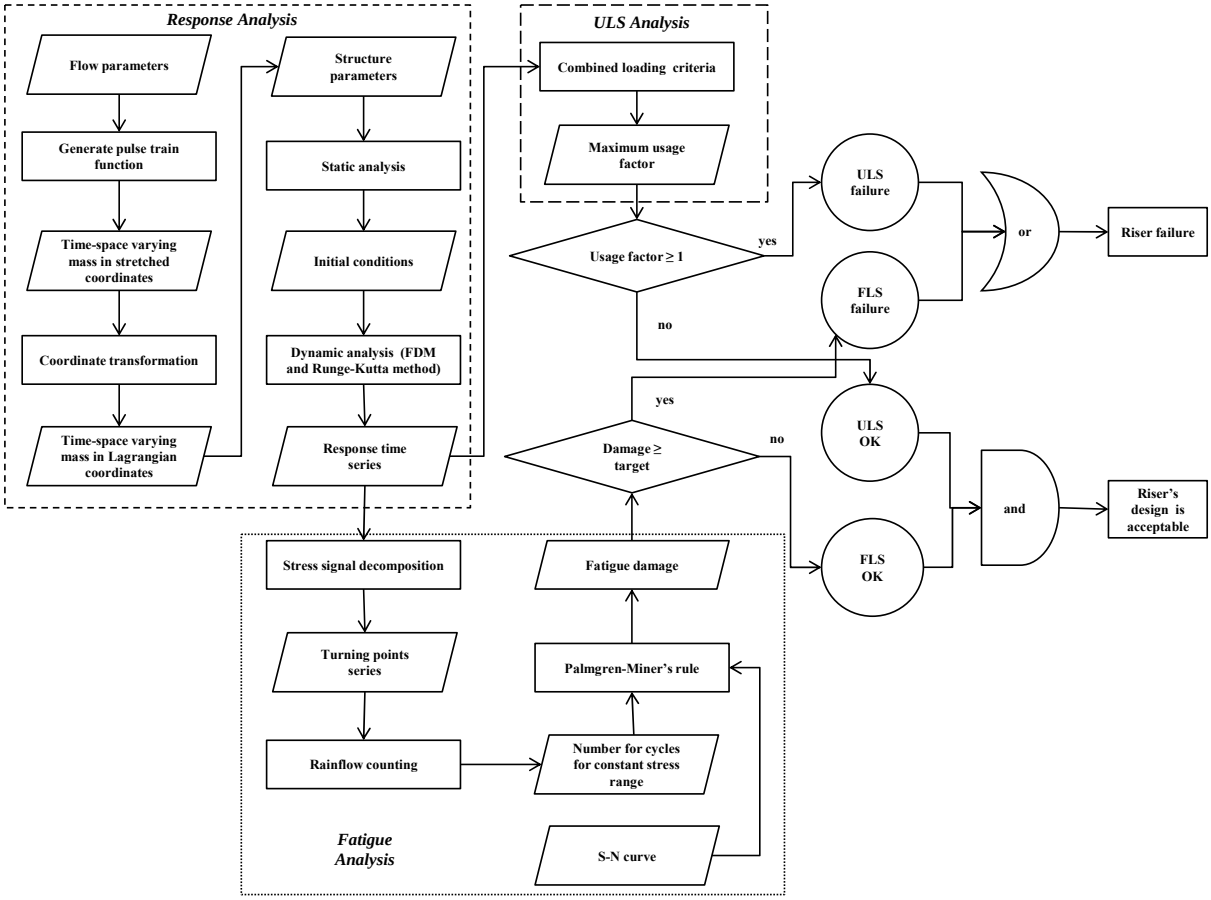

Fig. 2. Procedure for determining the response of a marine riser subjected to 2-FIV, for and assessing the ULS and FLS.

Firstly, the static configuration is calculated with the 'bvp4c' function in Matlab (Wang et al., 2015, 2014; Wang and Duan, 2015) and illustrated in Fig. 3, where a conveyed fluid of 400 kg·m^{-3} density (average density between oil and gas) has been assumed.

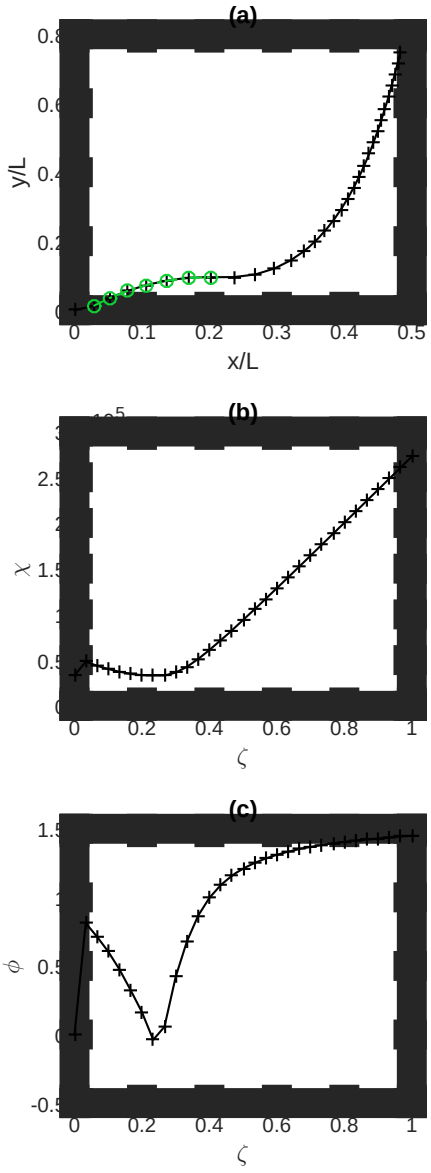

Fig. 3. Static configuration of **(b)** dimensionless effective tension and **(c)** inclination angle.

As a base case, we perform time-domain analyses for λ_l=1, which means that the liquid slug equals the riser's length, resembling a severe slugging situation. In addition, cases for λ_l=0.25 and λ_l=2 have also been studied. Moreover, the presumed relationship λ/λ_l=2 is used, which means that liquid slugs and gas bubbles have the same length. For the liquid

phase, 800 kg·m^{-3} density is used and zero density for the gas one. Regarding the conveyed fluid's velocity U, we have included cases from 1 to 32 m·s^{-1}. Keeping in mind that the maximum operating velocity for liquid and gas pipelines are 4.5 and 24 m·s^{-1}, respectively (Stewart, 2016), results for U >24 m·s^{-1} are merely speculative.

In Fig. 4, the frequency-response curves are presented for the dimensionless effective tension (χ) and for the dimensionless curvature (ϕ') as function of the slugging frequency calculated as $f_l = U/(\lambda L)$. These quantities were chosen due to their significance in the design and analysis of risers. They are constructed by using the above mentioned static configuration (see Fig. 3) as initial conditions for the first case of analysis in backward sweep of slugging frequencies and then in forward sweep, i.e. the flow velocity is progressively reduced while the solution from a previous time-domain analysis is used as initial conditions for the next one. Afterwards, the static configuration is employed again as initial conditions to carry out analyses in forward sweep. This procedure is followed in order to capture different responses at the same excitation frequency which could possibly happen in nonlinear systems.

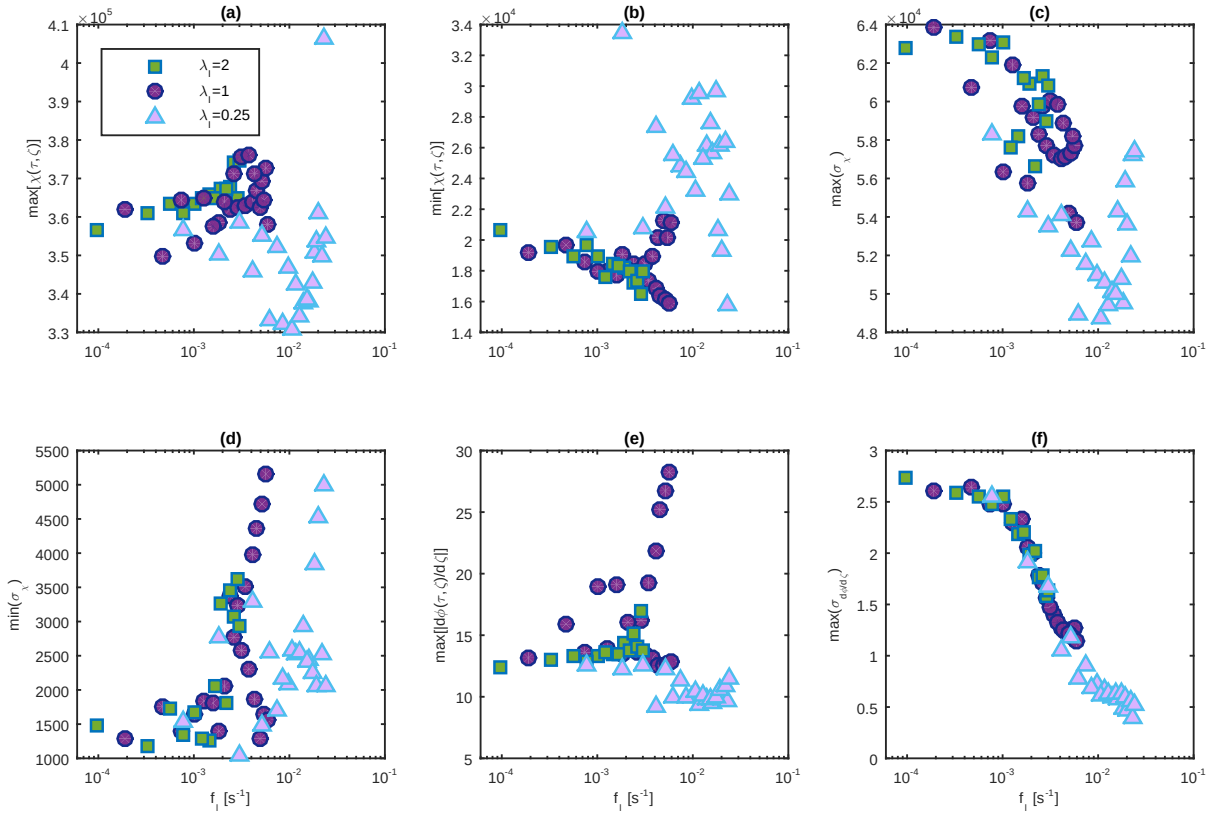

Fig. 4. Frequency-response curves for 2-FIV in a SLWR: **(a)** maximum dimensionless effective tension, **(b)** minimum dimensionless effective tension, **(c)** maximum standard deviation of dimensionless effective tension **(d)** minimum standard deviation of dimensionless effective tension, **(e)** maximum dimensionless curvature and **(f)** maximum standard deviation of dimensionless curvature.

Figures 4(a) and (e) show the maxima of the dimensionless effective tension and the dimensionless curvature, respectively, where high values are associated with the attainment of the ULS. Furthermore, one may be interested in the minimum effective tension in Fig. 4(b), where negative values would lead to the undesirable Euler buckling (Bai and Bai, 2005). This situation is not identified here. Figures 4(c) and (f), showing the maxima for standard deviation of responses along the length of the riser, provide information about the vibrations

excited by the slug flow. At low frequencies, the stiffness of the system is dominant, making the riser to follow the density waves of the conveyed fluid. As the slugging frequency increases, the motions are controlled by the riser's mass and the density waves lose their influence on the amplitude of the responses. Fig. 4(d) the minimum standard deviation for the effective tension grows with the increasing slugging frequency; however, the values are of low magnitude. Similar figure for the curvature is not needed since the applied boundary conditions impose the minimum standard deviation to be invariably zero.

To further analyse the riser dynamics, the following flow parameter pairs are considered: (λ_l=2, U =1 m·s^{-1}), (λ_l=1, U =15.5 m·s^{-1}), (λ_l=0.25, U =31.45 m·s^{-1}) and (λ_l =0.25, U =2.45 m·s^{-1}). The resulting motions are illustrated in Figs. 5, 6, 7 and 8, respectively. There, subfigures (a) and (b) present the structural velocity envelopes in the tangential and the normal directions, respectively. Subfigures (c) show the 3-D time histories for normal velocity. Subfigures (d), (i) and (j) are an attempt to illustrate the motions at the buoyancy section where the curvature is the largest; they show phase portraits, dimensionless curvature time histories and dimensionless curvature amplitude spectra, respectively. Subfigures (e) depict the phase portraits at the riser centre. Finally, subfigures (f), (g) and (h) display the phase portraits, dimensionless effective tension time histories and dimensionless effective tension amplitude spectra in the vicinity of the top end, where the tension is the highest.

One may infer the following from Figs. 5 through 8. At low slugging frequency and long slugs (see Fig. 5), the riser alternates between the liquid filled position and gas filled position. In the process, vibrations are excited at the frequency of excitation f_l, and also at the dependent frequencies $3f_l$ and $5f_l$. After some increase of slugging frequency and for

slugs of the size of the riser (see Fig. 6), the phase portraits get collapsed and the amplitude grows for both the axial velocity and tangential velocity. The amplitude spectra show major participation of the excited frequency f_l at the buoyancy section, and f_l and $3f_l$ at the top end. This state is associated with marked fatigue loads. For high slugging frequency and short length slugs (see Fig. 7), velocities are still high; however, the amplitudes of motions are relatively small, and not harmful for the fatigue life. Interesting dynamics are observed for short slugs at intermediate frequency (see Fig. 8). In this case, a new trajectory at the top end is observed in the phase portrait. Also, motions are dominated by the slugging frequency with lesser participation of the dependent frequencies.

A general thing to observe is that the SLWR develops large amplitude vibrations close to the bottom end, which is explained by two facts: one is the vast amount of energy which is extracted from the system throughout the path of the slug flow (Zhu et al., 2018), and another is the acceleration of the riser at the buoyancy section by the passing masses where substantial change of inclination angle occurs. This vibration pattern for 2-FIV is unequivocally different from the top-end imposed excitations, where the vibrations occur at the top end [see for example J. Wang et al. (2018)].

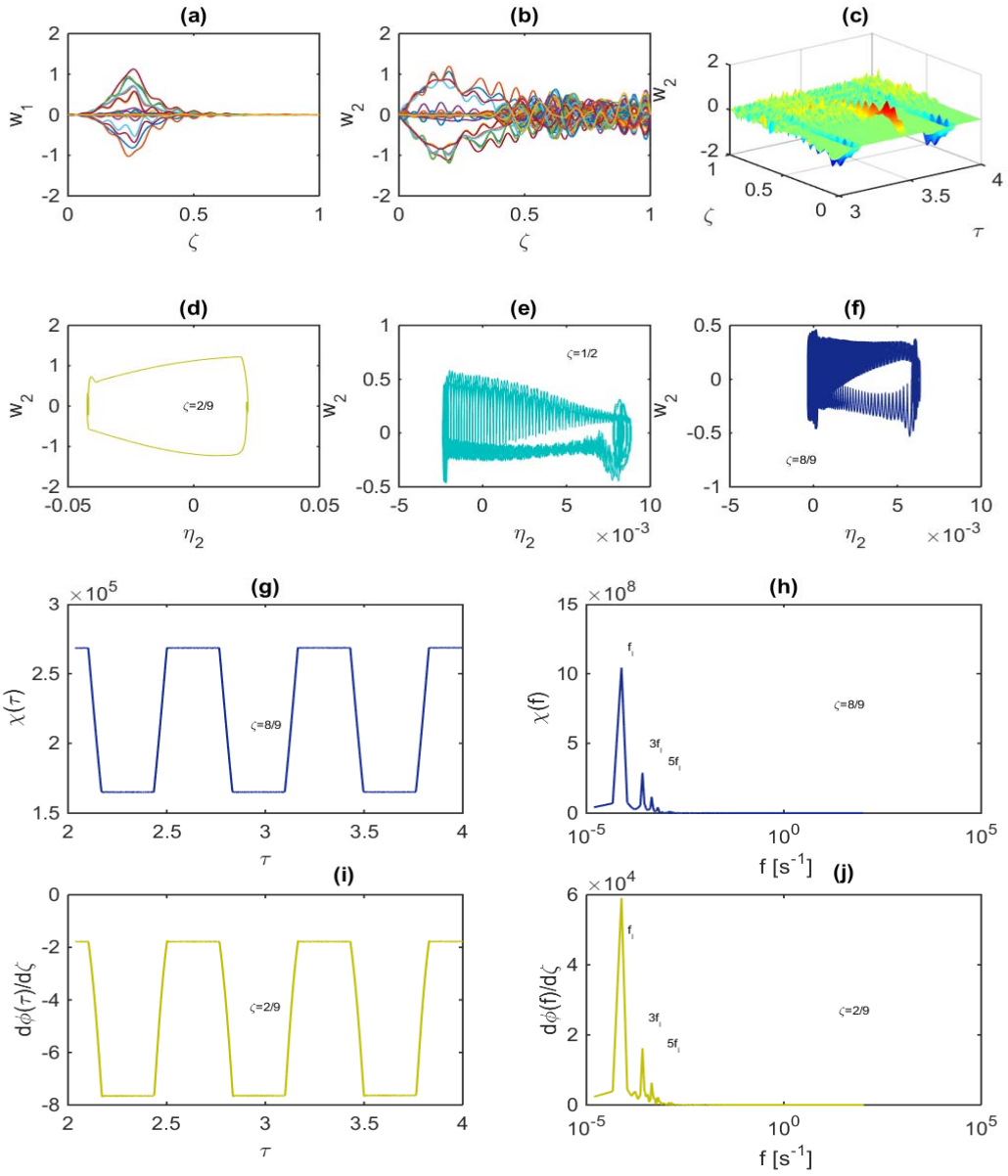

Fig. 5. Evolution of riser's response excited by low frequency long slugs (λ_1=2, U =1 m·s^{-1}, f_l =9.47×10^{-5} s^{-1}): **(a)** envelope of dimensionless tangential velocity, **(b)** envelope of dimensionless normal velocity, **(c)** time history of dimensionless normal velocity, **(d)** phase portrait of vibrations in normal direction at ζ =2/9, **(e)** phase portrait of vibrations in normal direction at ζ =1/2, **(f)** phase portrait of vibrations in normal direction at ζ =8/9, **(g)** dimensionless effective tension time history at ζ =8/9, **(h)** dimensionless effective tension spectrum at ζ =8/9, **(i)** dimensionless curvature time history at ζ =2/9 and **(j)** dimensionless curvature spectrum at ζ =2/9.

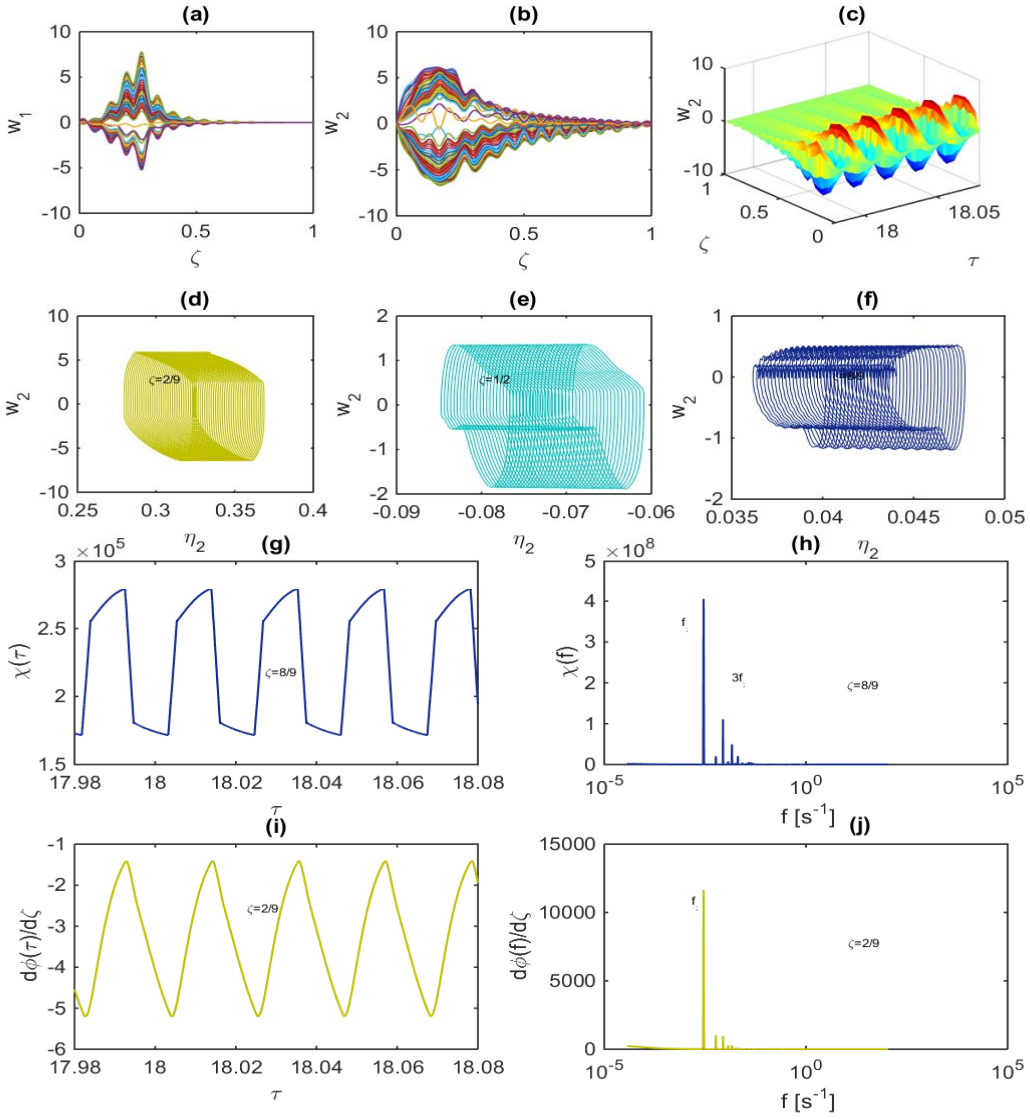

Fig. 6. Evolution of riser's response excited by intermediate length slugs at intermediate frequency (λ_l=1, U =15.5 m·s^{-1}, f_l=2.9×10^{-3} s^{-1}): **(a)** envelope of dimensionless tangential velocity, **(b)** envelope of dimensionless normal velocity, **(c)** time history of dimensionless normal velocity, **(d)** phase portrait of vibrations in normal direction at ζ =2/9, **(e)** phase portrait of vibrations in normal direction at ζ =1/2, **(f)** phase portrait of vibrations in normal direction at ζ =8/9, **(g)** dimensionless effective tension time history at ζ =8/9, **(h)** dimensionless effective tension spectrum at ζ =8/9, **(i)** dimensionless curvature time history at ζ =2/9 and **(j)** dimensionless curvature spectrum at ζ =2/9.

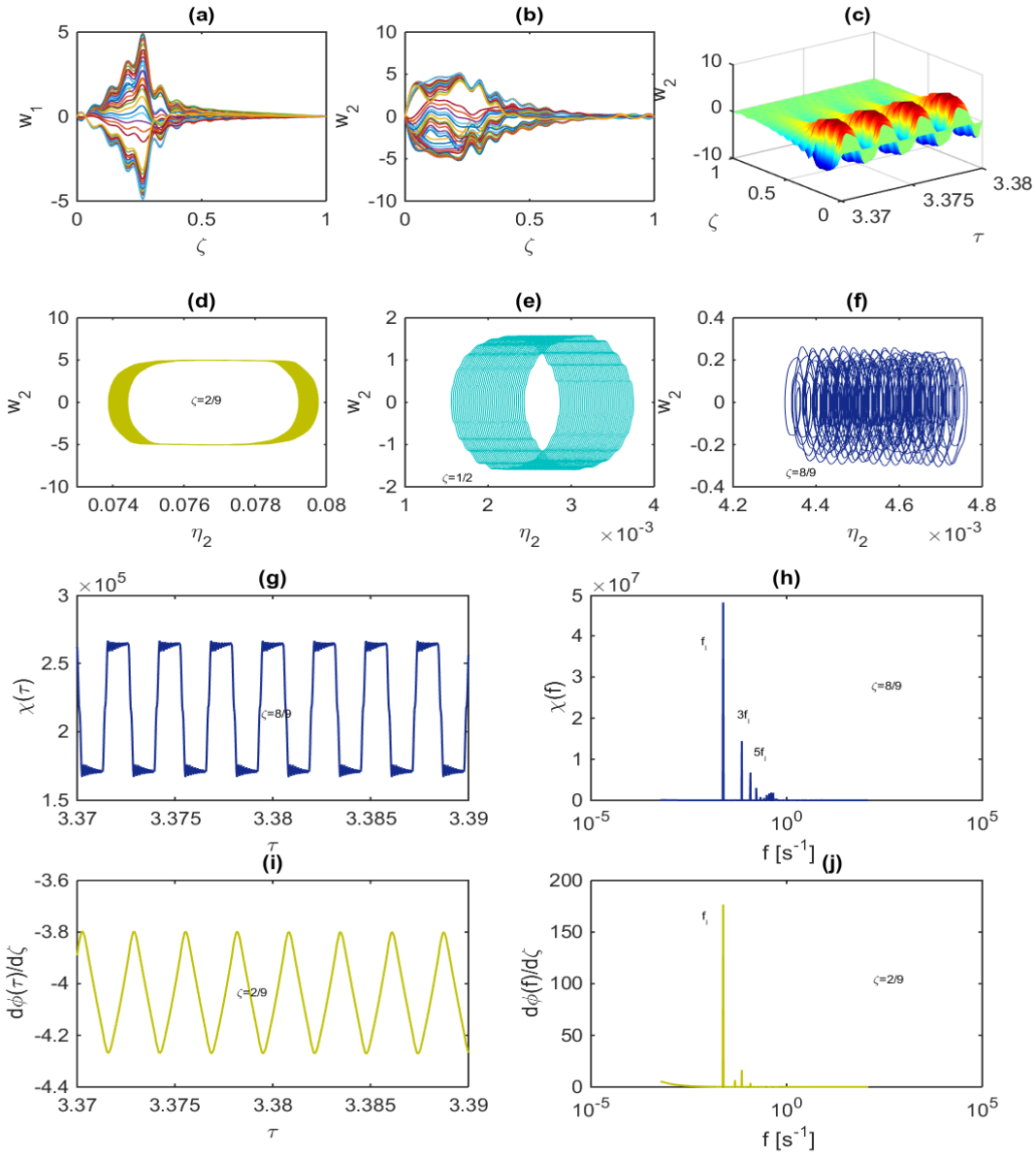

Fig. 7. Evolution of riser's response excited by high frequency short slugs (λ_l=0.25, U =31.45 m·s^{-1}, f_l =2.38×10^{-2} s^{-1}): **(a)** envelope of dimensionless tangential velocity, **(b)** envelope of dimensionless normal velocity, **(c)** time history of dimensionless normal velocity, **(d)** phase portrait of vibrations in normal direction at ζ =2/9, **(e)** phase portrait of vibrations in normal direction at ζ =1/2, **(f)** phase portrait of vibrations in normal direction at ζ =8/9, **(g)** dimensionless effective tension time history at ζ =8/9, **(h)** dimensionless effective tension spectrum at ζ =8/9, **(i)** dimensionless curvature time history at ζ =2/9 and **(j)** dimensionless curvature spectrum at ζ =2/9.

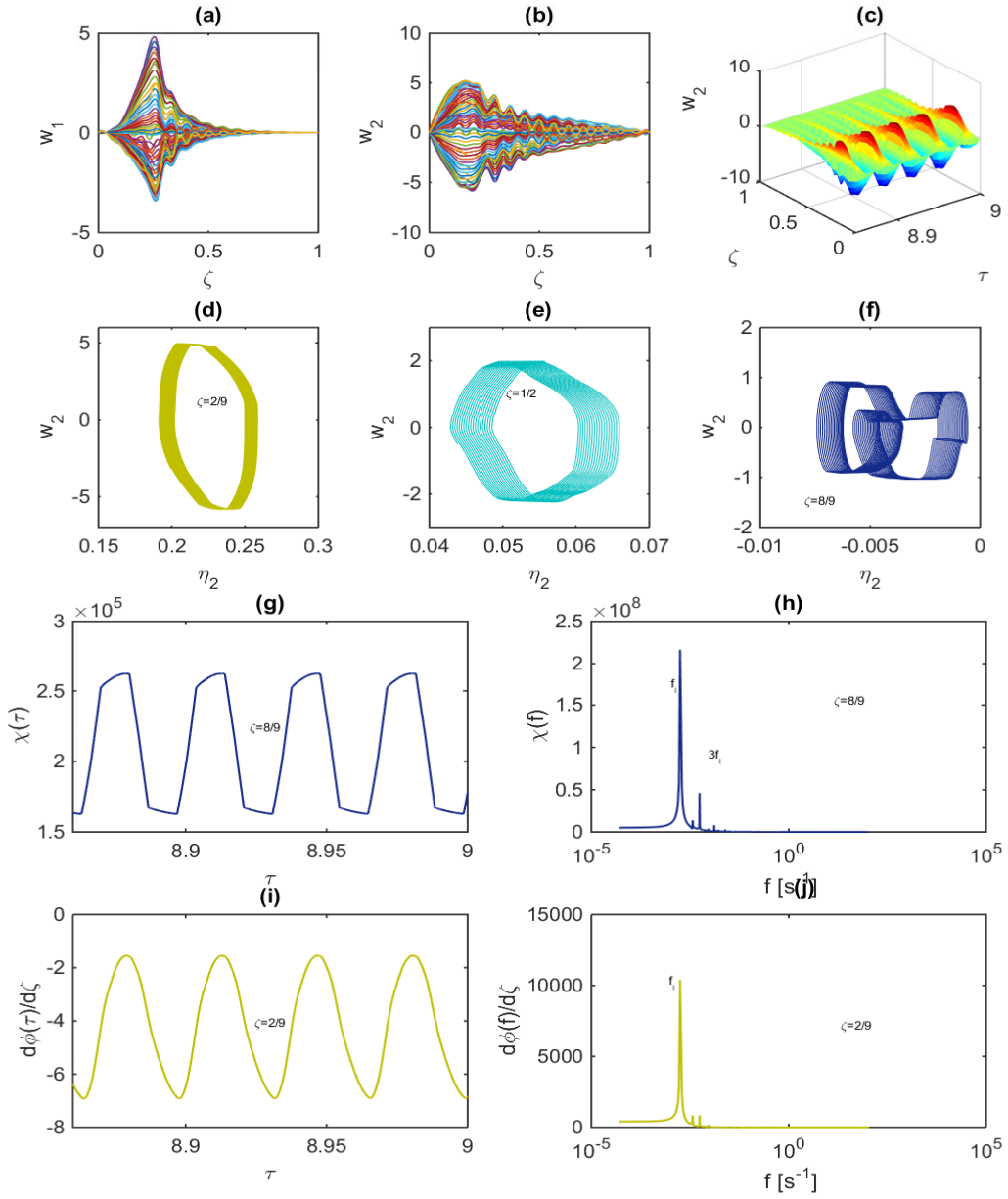

Fig. 8. Evolution of riser's response excited by slow short slugs (λ_l=0.25, U =2.45 m·s^{-1}, f_l =1.9×10^{-3} s^{-1}): **(a)** envelope of dimensionless tangential velocity, **(b)** envelope of dimensionless normal velocity, **(c)** time history of dimensionless normal velocity, **(d)** phase portrait of vibrations in normal direction at ζ =2/9, **(e)** phase portrait of vibrations in normal direction at ζ =1/2, **(f)** phase portrait of vibrations in normal direction at ζ =8/9, **(g)** dimensionless effective tension time history at ζ =8/9, **(h)** dimensionless effective tension spectrum at ζ =8/9, **(i)** dimensionless curvature time history at ζ =2/9 and **(j)** dimensionless curvature spectrum at ζ =2/9.

4. Limit state assessment

Like in other types of structures such as plated structures (Paik, 2018), methodologies for limit state analysis and design are also adopted for risers.

4.1 Ultimate limit state

4.1.1 Fundamentals of ULS analysis

We now investigate whether the 2-FIV can lead to the riser's failure by an ULS assessment (see Fig. 2). To judge the structural sufficiency in ULS, the local usage factors $\upsilon(\tau,\zeta)$ for combined loading criteria can be evaluated in the form of (DNV GL, 2018):

$$\upsilon = \begin{cases} \sqrt{\dfrac{|\mathcal{M}|}{\mathcal{M}_k}\sqrt{1-\left(\dfrac{p_i-p_e}{p_b}\right)^2}+\left(\dfrac{T_e}{T_k}\right)^2+\left(\dfrac{p_i-p_e}{p_b}\right)^2}, & p_i \geq p_e \\ \left\{\left[\dfrac{|\mathcal{M}|}{\mathcal{M}_k}+\left(\dfrac{T_e}{T_k}\right)^2\right]^2+\left(\dfrac{p_e-p_i}{p_c}\right)^2\right\}^{1/4}, & p_i < p_e \end{cases} \tag{17}$$

where $\mathcal{M} = EI\,\partial\phi/\partial s$ is the bending moment, $\mathcal{M}_k$ is the plastic bending moment resistance, p_i is the internal pressure, p_e is the external pressure, p_b is the burst resistance, T_k is the plastic axial force resistance and p_c is the hoop buckling capacity [for detailed definition of the variables, DNV GL (2018) is referred to]. One would not expect the riser to fail as long as $\upsilon(\tau,\zeta)$ is kept below one for all ζ and τ. Also, because design is not the aim of this work, the partial safety factors have all been taken as unity.

Equation (17) describes a ULS for load controlled conditions, which is usually the case for risers subjected to extreme sea environments. Said equation limits the occurrence of plastic deformations, hoop buckling or bursting. Alternatively, on could use structural checks for displacement controlled conditions, in which plastic strains can be allowed, for pipelines for instance; however, this is not the case for dynamic marine risers. Thus, Eq. (17) is a suitable formulation for the present problem.

4.1.2 Results for ULS

The time histories generated in Section 3 are analysed at every riser's coordinate and time, and the maximum usage factor is reported in Fig. 9.

Analysis of the results leads to the following conclusions. For the domain of analysis, the usage factors are all below one, and therefore, the riser will not fail for the ULS in any case. For long slugs, λ_l=2, a bifurcation in the calculated usage factors is visible at slugging frequencies above 2×10^{-3} s^{-1}, where the upper branch corresponds to forward sweep analyses and the lower one to backward sweep. Qualitatively equivalent results are obtained for λ_l=1. For this case however, the upper branch rises to higher, possibly dangerous usage factors. Regarding short slugs of λ_l =0.25, the factors are concentrated in a single branch for frequencies in the order of 1×10^{-2} s^{-1}, whereas scatter is observed at lower frequencies.

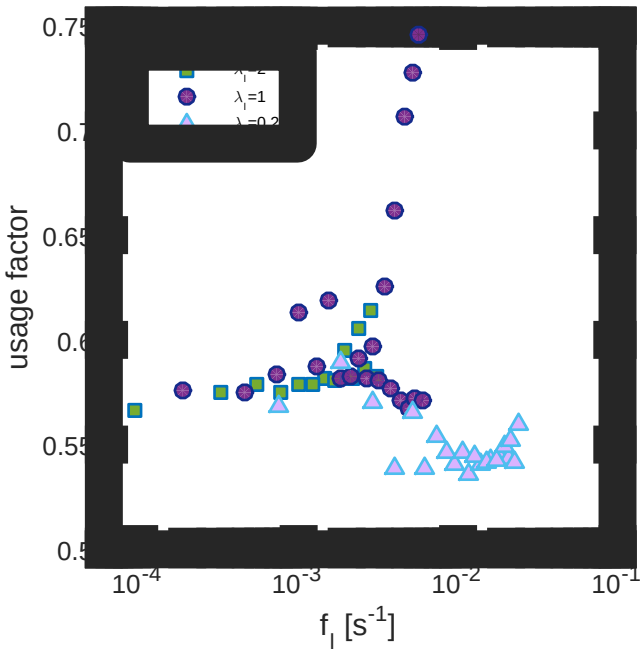

Fig. 9. Calcul

frequencies an

4.2 Fatigue

4.2.1 Fundan

The ris

in turn generat

damage approa

First, we assemble the time history of normal stress S at each node, composed of the linear combination of axial stress due to tension and bending stress, i.e. (DNV GL, 2018):

$$S = \frac{T_e}{\pi(D-h)h} + \frac{32\mathcal{M}(D-h)}{\pi\left[D^4-(D-2h)^4\right]}, \tag{18}$$

where D is the structural diameter of the riser and h is the pipe wall thickness.

Then, each stress signal $S(t,s)$ is decomposed into a series of turning points. They are subsequently analysed by means of the rainflow counting algorithm, for which we find useful the Matlab toolbox developed by Niesłony (2009). The number of cycles for various stress ranges n_i is obtained.

Lastly, the Palmgren-Miner's rule is employed to estimate the fatigue damage in the form of:

$$\mathcal{D} = \sum_{i=1}^{k} \frac{n_i}{N_i}, \tag{19}$$

where $\mathcal{D}$ is the accumulated fatigue damage and N_i is the number of cycles to failure at constant stress range. The last is evaluated from an existing S-N curve (DNV GL, 2016). Because the hypothetical SLWR was originally analysed by using the D type S-N curve (Felisita et al., 2017), the same curve is also employed in the calculations of this work. One could say that the structure can withstand the dynamic loads throughout its envisaged life as much as the fatigue damage $\mathcal{D}$ is kept below one.

4.2.2 Results for fatigue analysis

The calculated fatigue damage per year is reported in Fig. 10. The damage occurs mostly at low slugging frequencies and becomes acute at f_l=2.1×10^{-3} s^{-1}. Then, it turns out to be practically unnoticeable for frequencies above 3.5×10^{-3} s^{-1}, or in terms flow velocity U, one may not expect fatigue issues for U above 34, 18 and 4.6 m·s^{-1} for slug lengths λ_l of 2, 1 and 0.25, respectively. Scenarios with high fatigue damage are illustrated in Figs. 6 and 8.

It is observed that the maximum fatigue damage per year caused by 2-FIV is in the order of 0.028, which could be higher than the one caused by waves. To have an idea, waves can cause fatigue damage per year of 0.001 in a SLWR (Felisita et al., 2017) and from 0.0013 to 0.004 at the TDP in a steel catenary riser (SCR) when considering a linear stiffness soil model (Elosta et al., 2014). On the other hand, slugging happens mostly at the end of the service life for hydrocarbon facilities, and therefore, the total cumulative fatigue damage can be kept under acceptable levels.

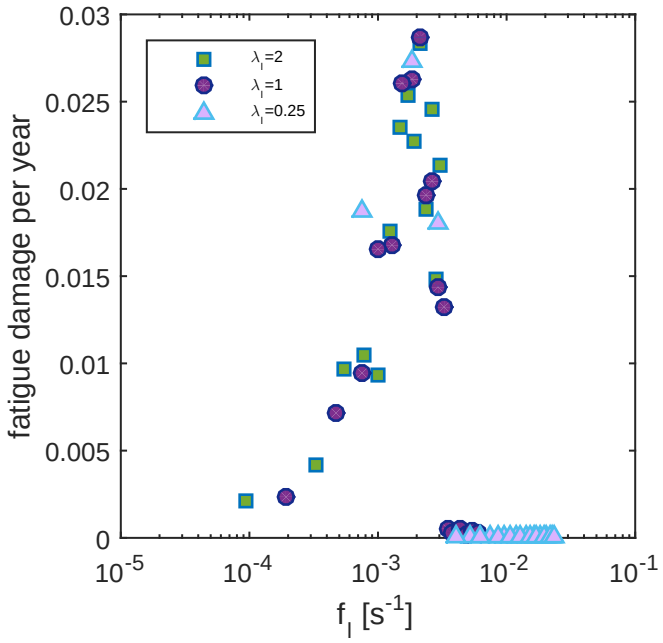

Fig. 10. Calcu

frequencies anc

5. Concluding remarks

This paper has focused on the 2-FIV in marine risers and to understand whether this phenomenon could be detrimental for the ULS and FLS. For this purpose, a SLWR has been modelled as an Euler-Bernoulli beam and the internal fluid as a plug-flow with time-space-varying mass in the form of a rectangular pulse train. The governing system of equations has been solved by means of the finite difference method and the Runge-Kutta method. Then, various scenarios of severe slugging were analysed in the time-domain. Results in the form of phase portraits, time histories, velocity envelopes, and frequency amplitude spectra show that the riser's tangential and normal velocities have major amplitude in the region close to the bottom end. Assessment of relevant limit states indicates that the 2-FIV may not cause failure of the riser for ULS and the fatigue damage per year can be as high as 0.03 for FLS.

Based on this study, it is a reasonable design choice to consider the 2-FIV phenomenon for both the ULS and FLS. However, it may still be worth discussing whether real slug flows can exist with the parameters here found as critical. First, the slug flow pattern is rather an irregular density wave and not a rectangular wave. Secondly, as the riser vibrates, the path of the internal flow is constantly changed, and thus, the flow pattern could be modified. Moreover, the environmental loads from waves, currents and floater motions may also modify the said flow path, generally amplifying the motions (Chatjigeorgiou, 2017; Ortega et al., 2017). To investigate the said issues, further research should be conducted with robust models, numerical methods and experimental methods. Also, it is advisable to develop methodologies to assess the safety of risers subjected to 2-FIV. In the case of the authors, we are interested in investigating the applicability of the rectangular pulse train mass model in comparison to realistic irregular density flows by using a multiphase flow simulator. Also, we would like to conduct experiments, which results would represent a valuable contribution.

It could be said that this work has fulfilled its aim to understand the influence of the 2-FIV on the riser's dynamics, ULS and FLS.

Acknowledgements

This study was undertaken at the Korea Ship and Offshore Research Institute at Pusan National University which has been a Lloyd's Register Foundation Research Centre of Excellence since 2008. This work was supported by a 2-Year Research Grant of Pusan National University. The first author would like to acknowledge the scholarship from the Mexican National Council for Science and Technology (CONACYT) (scholarship number 409711). The authors are grateful to Ing. Víctor Hugo Pérez Robles for his valuable discussion on flows inside oil and gas pipelines.

References

Abdulkadir, M., Hernandez-Perez, V., Lowndes, I.S., Azzopardi, B.J., Dzomeku, S., 2014. Experimental study of the hydrodynamic behaviour of slug flow in a vertical riser. Chem. Eng. Sci. 106, 60–75.

Adefemi, I.O., Kara, F., Okereke, N.U., 2017. Investigation of slug mitigation: self-lifting approach in a deepwater oil field. Underw. Technol. 34 (4), 157–169.

Ai, S., Xu, Y., Kang, Z., Yan, F., 2018. Performance comparison of stress-objective and fatigue-objective optimization for steel lazy wave rrisers. Ships and Offshore Structures, doi.org/10.1080/17445303.2018.1522054.

An, C., Su, J., 2015. Dynamic behavior of pipes conveying gas-liquid two-phase flow. Nucl. Eng. Des. 292, 204–212.

Bai, Y., Bai, Q., 2005. Chapter 22 - Design of Deepwater Risers, in: Subsea Pipelines and Risers. Elsevier Ltd, Oxford, UK, pp. 401–412.

Bai, X., Vaz, M.A., Morooka, C.K., Xie, Y., 2017. Dynamic tests in a steel catenary riser reduced scale model. Ships and Offshore Structures, 12(8): 1064-1076.

Bai, Y., Xie, W., Gao, X., Xu, W., 2018. Dynamic analysis of a cantilevered pipe conveying fluid with density variation. J. Fluids Struct. 81, 638–655.

Bai, Y., Zhang, D., Zhu, K., Zhang, T., 2018. Dynamic analysis of umbilical cable under interference with riser. Ships and Offshore Structures, 13(8): 809-821.

Cabrera-Miranda, J.M., Paik, J.K., 2018. Long-term stochastic heave-induced dynamic buckling of a top-tensioned riser and its influence on the ultimate limit state reliability. Ocean Eng. 149, 156–169.

Chatjigeorgiou, I.K., 2017. Hydroelastic response of marine risers subjected to internal slug-flow. Appl. Ocean Res. 62, 1–17.

Chatjigeorgiou, I.K., 2010a. Three dimensional nonlinear dynamics of submerged, extensible catenary pipes conveying fluid and subjected to end-imposed excitations. Int. J. Non. Linear. Mech. 45 (7), 667–680.

Chatjigeorgiou, I.K., 2010b. On the effect of internal flow on vibrating catenary risers in three dimensions. Eng. Struct. 32 (10), 3313–3329.

Chatjigeorgiou, I.K., 2008. A finite differences formulation for the linear and nonlinear dynamics of 2D catenary risers. Ocean Eng. 35 (7), 616–636.

Cheng, J., Cao, P., 2013. Design of Steel Lazy Wave Riser for Disconnectable FPSO, in: Offshore Technology Conference (OTC). Houston, Texas, USA, OTC 24166.

DNV GL, 2018. DNVGL-ST-F201: Dynamic risers. Høvik, Norway.

DNV GL, 2016. DNVGL-RP-C203: Fatigue Design of Offshore Steel Structures. Høvik, Norway.

Dong, L., Huang, Y., Zhang, Q., Liu, G., 2012. Taper design and non-linear analysis of bend stiffeners at the riser-vessel interface. Ships and Offshore Structures, 8(2): 189-199.

Elosta, H., Huang, S., Incecik, A., 2014. Wave loading fatigue reliability and uncertainty analyses for geotechnical pipeline models. Ships Offshore Struct. 9 (4), 450–463.

Felisita, A., Gudmestad, O.T., Karunakaran, D., Martinsen, L.O., 2017. Review of Steel Lazy Wave Riser Concepts for the North Sea. J. Offshore Mech. Arct. Eng. 139 (1), 011702-1-011702-15.

Fokin, B.S., Gotovskii, M.A., Belen'kii, M.Y., Mukhina, I.S., 2006. The parameters of a two-phase flow at which the occurrence of an intermittent flow pattern in vertical tubes is ruled out. Therm. Eng. 53 (1), 839–841.

Fujita, K., 1990. Flow-induced vibration and fluid-structure interaction in nuclear power plant components. J. Wind Eng. Ind. Aerodyn. 33 (1–2), 405–418.

Gao, Y., Fu, S., Ma, L., Chen, Y., 2014. Experimental investigation of the response performance of VIV on a flexible riser with helical strakes. Ships and Offshore Structures, 11(2): 113-128.

Gao, Y., Yang, J., Xiong, Y., Wang, M., Lu, D., 2016. VIV response of a long flexible riser fitted with different helical strake coverages in uniform and linearly sheared currents.

Ships and Offshore Structures, 12(4): 575-590.

Gong, J., Yang, Z., Ma, L., Wang, P., 2014. Severe slugging in air-water hybrid riser system. Adv. Mech. Eng. 2014.

Gu, J., Dai, B., Wang, Y., Li, M., Duan, M., 2017. Dynamic analysis of a fluid-conveying pipe under axial tension and thermal loads. Ships and Offshore Structures, 12(2): 262-275.

Gulyayev, V.I., Tolbatov, E.Y., 2004. Dynamics of spiral tubes containing internal moving masses of boiling liquid. J. Sound Vib. 274 (1–2), 233–248.

Guo, L., Duan, M., Wang, Y., Yu, F., 2013. Experimental investigation on dynamic model testing of a deep-water riser support by truncated hybrid method. Ships and Offshore Structures, 9(3): 344-353.

Han, P., Guo, L., 2015. Numerical simulation of terrain-induced severe slugging coupled by hydrodynamic slugs in a pipeline-riser system. Int. J. Heat Fluid Flow 56, 355–366.

Hara, F., 1977. Two-Phase-Flow-Induced Vibrations in a Horizontal Piping System. Bull. JSME 20 (142), 419–427.

Hara, F., Yamashita, T., 1978. Parallel Two-Phase-Flow-Induced Vibrations in Fuel Pin Model. J. Nucl. Sci. Technol. 15 (5), 346–354.

Hirdaris, S.E., Bai, W., Dessi, D., Ergin, A., Gu, X., Hermundstad, O.A., Huijsmans, R., Iijima, K., Nielsen, U.D., Parunov, J., Fonseca, N., Papanikolaou, A., Argyriadis, K., Incecik, A., 2014. Loads for use in the design of ships and offshore structures. Ocean Eng. 78, 131–174.

Hirdaris, S.E., Lees, A.W., 2005. A conforming unified finite element formulation for the

vibration of thick beams and frames. Int. J. Numer. Methods Eng. 62 (4), 579–599.

Hoffman, J., Yun, H., Modi, A., Pearce, R., 2010. Parque das Conchas (BC-10) Pipeline , Flowline and Riser System Design, Installation and Challenges, in: Offshore Technology Conference (OTC). Houston, Texas, USA, OTC 20650.

Jia, D., 2012. Slug Flow Induced Vibration in a Pipeline Span, a Jumper, and a Riser Section, in: Offshore Technology Conference. Houston, Texas, USA, OTC 22935.

Kadri, U., Henkes, R.A.W.M., Mudde, R.F., Oliemans, R.V.A., 2011. Effect of gas pulsation on long slugs in horizontal gas-liquid pipe flow. Int. J. Multiph. Flow 37 (9), 1120–1128.

Katifeoglou, S.A., Chatjigeorgiou, I.K., Dynamics of shell-like tubular segments at the sagbend region of a steel caternary riser. Ships and Offshore Structures, 11(8): 860-873.

Khan, R.A., Ahmad, S., 2017. Nonlinear dynamic and bilinear fatigue reliability analyses of marine risers in deep offshore fields. Ships and Offshore Structures, 13(1): 10-19.

Kim, S., Kim, M.-H., 2015. Dynamic behaviors of conventional SCR and lazy-wave SCR for FPSOs in deepwater. Ocean Eng. 106, 396–414.

Kuiper, G.L., Brugmans, J., Metrikine, A. V., 2008. Destabilization of deep-water risers by a heaving platform. J. Sound Vib. 310 (3), 541–557.

Li, F., Cao, J., Duan, M., An, C., Su, J., 2016. Two-phase Flow Induced Vibration of Subsea Span Pipeline, in: Proceedings of the Twenty-Sixth (2016) International Ocean and Polar Engineering Conference. Rhodes, Greece, pp. 1153–1160.

Li, W., Guo, L., Xie, X., 2017. Effects of a long pipeline on severe slugging in an S-shaped riser. Chem. Eng. Sci. 171, 379–390.

Li, F.Z., Low, Y.M., 2012. Influence of low-frequency vessel motions on the fatigue response of steel catenary risers at the touchdown point. Ships and Offshore Structures, 9(2): 134-148.

Lou, M., Chen, P., Chen, Z., 2016. Experimental investigation on the suppression of vortex-induced vibration of two interfering risers by control rods. Ships and Offshore Structures, 12(8): 1117-1126.

Lu, Y., Liang, C., Manzano-Ruiz, J.J., Janardhanan, K., Perng, Y.-Y., 2016. Flow-Induced Vibration in Subsea Jumper Subject to Downstream Slug and Ocean Current. J. Offshore Mech. Arct. Eng. 138 (2), 021302-1-021302-10.

Ma, T., Gu, J., Duan, M., 2017. Dynamic response of pipes conveying two-phase flow based on Timoshenko beam model. Mar. Syst. Ocean Technol. 12 (3), 196–209.

Miwa, S., Mori, M., Hibiki, T., 2015. Two-phase flow induced vibration in piping systems. Prog. Nucl. Energy 78, 270–284.

Moore, B., Easton, A., Cabrera, J., Webb, C., George, B., 2017. Stones Development: Turritella FPSO - Design and Fabrication of the World's Deepest Producing Unit, in: Offshore Technology Conference (OTC). Houston, Texas, USA, OTC-27663-MS.

Niesłony, A., 2009. Determination of fragments of multiaxial service loading strongly influencing the fatigue of machine components. Mech. Syst. Signal Process. 23 (8), 2712–2721.

Onuoha, M.D.U., Duan, M., Wang, Y., 2016. Dynamic Response and Stress Impact Analysis of Production Riser under Severe Slug Flow, in: Proceedings of the Twenty-Sixth (2016) International Ocean and Polar Engineering Conference. Rhodes, Greece, pp. 175–184.

Onuoha, M.D.U., Li, Q., Duan, M., Gao, Q., 2018. Severe slugging in deepwater risers: A coupled numerical technique for design optimisation. Ocean Eng. 152, 234–248.

Ortega, A., Rivera, A., Larsen, C.M., 2017. Slug Flow and Waves Induced Motions in Flexible Riser. J. Offshore Mech. Arct. Eng. 140 (1), 011703-1–011703-9.

Ortega, A., Rivera, A., Nydal, J., Larsen, C.M., 2012. On the dynamic response of flexible risers caused by internal slug flow, in: Proceedings of the ASME 2012 31st International Conference on Ocean, Offshore and Arctic Engineering OMAE2012. Rio de Janeiro, Brazil, OMAE2012-83316.

Ortiz-Vidal, L.E., Mureithi, N.W., Rodriguez, O.M.H., 2017. Vibration response of a pipe subjected to two-phase flow : Analytical formulations and experiments. Nucl. Eng. Des. 313, 214–224.

Paidoussis, M.P., 2014. Pipes Conveying Fluid: Linear Dynamics I, in: Fluid-Structure Interactions Volume 1: Slender Structures and Axial Flow. Academic Press, Oxford, UK, pp. 63–233.

Paik, J.K., 2018. Ultimate Limit State Analysis and Design of Plated Structures. Second ed., John Wiley & Sons, Chichester, UK.

Park, K.S., Kim, Y.T., Kim, D.K., Yu, S.Y., Choi, H.S., 2015. A new method for strake configuration design of steel caternary risers. Ships and Offshore Structures, 11(4): 385-404.

Park, C.Y., Lee, S.J., Park, S.H., 2018. Experimental investigation of vortex- and wake-induced vibrations of tandom cylinders. Ships and Offshore Structures, 13(8): 877-884.

Stewart, M., 2016. Choosing a line size and wall thickness, in: Surface Production

Operations—Facility Piping and Pipeline Systems, Volume III. Gulf Professional Publishing, Waltham, MA, USA.

Tshuva, M., Barnea, D., Taitel, Y., 1999. Two-phase flow in inclined parallel pipes. Int. J. Multiph. Flow 25 (6–7), 1491–1503.

van der Heijden, B., Smienk, H., Metrikine, A. V, 2014. Fatigue analysis of subsea jumpers due to slug flow, in: Proceedings of the ASME 2014 33rd International Conference on Ocean, Offshore and Arctic Engineering OMAE2014. San Francisco, California, USA, OMAE2014-23146.

Vendhan, C.P., 2014. Coupled dynamics of deepwater structures - issues and challenges. Ships and Offshore Structures, doi.org/10.1080/17445302.2014.944334.

Wang, J., Duan, M., 2015. A nonlinear model for deepwater steel lazy-wave riser configuration with ocean current and internal flow. Ocean Eng. 94, 155–162.

Wang, J., Duan, M., He, R., 2018. A nonlinear dynamic model for 2D deepwater steel lazy-wave riser subjected to top-end imposed excitations. Ships Offshore Struct. 13 (3), 330–342.

Wang, J., Duan, M., He, T., Jing, C., 2014. Numerical solutions for nonlinear large deformation behaviour of deepwater steel lazy-wave riser. Ships Offshore Struct. 9 (6), 655–668.

Wang, J., Duan, M., Wang, Y., Li, X., Luo, J., 2015. A nonlinear mechanical model for deepwater steel lazy-wave riser transfer process during installation. Appl. Ocean Res. 50, 217–226.

Wang, J., Fu, S., Baarholm, R., Zhang, M., Liu, C., 2018. Global motion reconstruction of a

steel catenary riser under vessel motion. Ships and Offsshore Structures, doi.org/10.1080/17445302.2018.1500785.

Wang, L., Yang, Y., Liu, C., Li, Y., Hu, Q., 2018. Numerical investigation of dynamic response of a pipeline-riser system caused by severe slugging flow. Int. J. Press. Vessel. Pip. 159, 15–27.

Xing, L., Yeung, H., Shen, J., Cao, Y., 2013. Numerical study on mitigating severe slugging in pipeline/riser system with wavy pipe. Int. J. Multiph. Flow 53, 1–10.

Xu, J., Wang, D., Huang, H., Duan, M., Gu, J., An, C., 2017. A vortex-induced vibration model for the fatigue analysis of a marine drilling riser. Ships and Offshore Structures, 12(Sup1): S280-S287.

Yan, K., Ge, P., Hong, J., 2013. Experimental study of shell side flow-induced vibration of conical spiral tube bundle. J. Hydrodyn. 25 (5), 695–701.

Ye, M., Duan, M., Li, M., Chen, J., Tian, K., Han, F., Hu, Z., 2014. An active trunction method for simulating deep-water riser installation. Ships and Offshore Structures, 9(6): 619-632.

Yuan, Y.C., Xue, H.X., Tang, W.Y., 2017. Added mass variation effect on vortex-induced vibration for flexible risers based on force-decomposition model. Ships and Offshore Structures, 13(Sup1): 1-12.

Zhang, Y., Duan, M., Wang, Y., Chu, G., 2015. Analytical study of the strength of adhesive joints of riser pipes. Ships and Offshore Structures, 10(4): 545-553.

Zhu, H., Gao, Y., Zhao, H., 2018. Experimental investigation on the flow-induced vibration of a free-hanging flexible riser by internal unstable hydrodynamic slug flow. Ocean Eng.

164, 488–507.